PCCP

PAPER

Check for updates

Cite this: *Phys. Chem. Chem. Phys.*, 2022, **24**, 28429

Improving carrier separation at the $TiO_2/CsPbIBr_2$ interface by gradient Sn-doping

Yingfeng Li, Bingxin Wang, Yingjian Liu, Wenxiang Gao and Meicheng Li *

Received 17th August 2022,
Accepted 31st October 2022

DOI: 10.1039/d2cp03781e

rsc.li/pccp

Subhani *et al.* found that Sm-doping in $CsPbIBr_2$ decreased its bandgap from 2.05 eV to 1.8 eV; thus, the efficiency of $CsPbIBr_2$ solar cells was improved by ~30%. However, Sm is a vital strategic resource with high costs. Metal Sn is much more abundant and cheaper than Sm; meanwhile, it has been proven that Sn can adjust the bandgap of $CsPbIBr_2$ in a broader range, 2.05 eV to 1.64 eV. Therefore, Sn-doping in $CsPbIBr_2$ may improve the efficiency of $CsPbIBr_2$ solar cells, even to a greater extent. In this work, we established the $TiO_2/CsPbIBr_2$ interface model by gradient Sn-doping in $CsPbIBr_2$ and investigated the impacts of such gradient doping on the carrier separation behaviors at the $TiO_2/CsPbIBr_2$ interface from the aspects of the cross-interface electric field, bandgap, and band matching, based on first-principles calculations. It is found that gradient Sn-doping can transfer more electrons from TiO_2 to perovskites, thus creating an enhanced cross-interface electric field conducive to the separation of carriers at the $TiO_2/CsPbIBr_2$ interface. Affected by the existence of the interface, the bandgap of each perovskite layer gradually increases as it moves away from the interface; in addition, due to the gradient Sn-doping, the steps between the bandgaps of adjacent perovskite layers become smaller and more uniform, which is favorable for the separation of electrons. In summary, gradient Sn-doping can improve the carrier separation at the $TiO_2/CsPbIBr_2$ interface.

1. Introduction

In recent years, organic–inorganic halide perovskite solar cells (PSCs) have made outstanding achievements.[2–4] The highest certified photoelectric conversion efficiency (PCE) has reached 25.7%.[5] However, the commercial development of organic–inorganic hybrid PSCs is severely limited by their instability.[6–9] All-inorganic cesium-based perovskite materials show much better stability than organic–inorganic hybrid perovskites.[10] Meanwhile, their bandgaps ranging from 1.3 to 2.4 eV[11,12] are also very suitable for fabricating solar cells. Therefore, all-inorganic cesium-based PSCs have been widely studied during these years.[13–17]

The most commonly used cesium-based perovskites are $CsPbI_xBr_{3-x}$. Of them, $CsPbI_3$ has the most suitable bandgap of ~1.73 eV, and the PCE of $CsPbI_3$-based PSCs has reached 19.03%.[13] But $CsPbI_3$ will undergo a phase transition at room temperature and thus is unstable.[14] $CsPbI_2Br$ is unstable under air conditions.[15,16] $CsPbBr_3$ shows desirable stability but has a large bandgap of ~2.3 eV, limiting its light absorption in the visible region. Only $CsPbIBr_2$ combines stability with an appropriate bandgap of ~2.05 eV and thus is most suitable for fabricating solar cells.

However, the PCE of $CsPbIBr_2$-based PSCs is not as high as expected.[17] The main reasons limiting the PCE of PSCs based on $CsPbIBr_2$ include its large bandgap, the mismatch between its band structure and that of the electron transport layer (ETL), and plenty of defects at the ETL/perovskite interface. Many general methods could tune the electronic properties of materials, *e.g.*, by introducing defects[18] or heteroatom-doping.[19] Subhani *et al.* have used $SmBr_3$ to modify the interface of TiO_2/perovskite.[1] They found that Sm-doping could passivate the interface and improve the crystallization of the perovskite layer. Meanwhile, based on first-principles calculations, they discovered that Sm-doping could reduce the bandgap of $CsPbIBr_2$, thus expanding the light absorption range. As a result, the PCE of Sm-doped $CsPbIBr_2$ PSCs reached 10.88% under one sun illumination.

In first-principles calculations in Subhani *et al.*'s report, Sm is distributed uniformly in $CsPbIBr_2$;[1] however, as evidenced by energy dispersive X-ray analysis, Sm should form a gradient doping within $CsPbIBr_2$. Such gradient doping may bring additional effects, such as introducing a gradient energy bandgap and an extra built-in electric field which can help inhibit the non-radiative recombination. It is of great significance in exploring the improvement mechanism of gradient doping on the performance of $CsPbIBr_2$-based PSCs.[20]

State Key Laboratory of Alternate Electrical Power System with Renewable Energy Sources, North China Electric Power University, Beijing, 102206, China.
E-mail: mcli@ncepu.edu.cn

Metal Sn is a much more abundant element on earth, thus much cheaper than Sm. In recent years, Sn-doping has also been widely used in improving the performance of $CsPbIBr_2$-based PSCs.[21–23] It has been found that Sn-doping can also narrow the bandgap of $CsPbIBr_2$, improving the morphology of the perovskite layer and reducing the interface defects. However, no matter in the experimental or the first-principles calculation research, the effect of the "gradient" Sn-doping on the carrier separation behaviors at the TiO_2/perovskite interface was not considered in detail.

This work investigated the cross-interface electric field, bandgap, and bands matching at the TiO_2/gradient Sn-doped $CsPbIBr_2$ interface based on first-principles calculations. It is found that gradient Sn-doping could transfer more electrons from TiO_2 to perovskites, thus creating an enhanced cross-interface electric field conducive to the separation of carriers. Meanwhile, the band energy structures of $CsPbIBr_2$ at the TiO_2/$CsPbIBr_2$ interface will be affected by both the existence of the interface and the gradient Sn-doping, and the gradient Sn-doping will bring minor and more uniform energy steps in the conductive band energy levels between adjacent $CsPbIBr_2$ layers, which is favorable for the separation of electrons.

2. Computational details

The cubic phase $CsPbIBr_2$ and rutile phase TiO_2 with experimental lattice parameters were used in building the interface model. According to the recent report,[1] the $CsPbIBr_2$(001) plane can contact the TiO_2(110) plane. So next, we built the models of $CsPbIBr_2$(001) and TiO_2 (11) slabs. The Sn-doping strategy must be determined first in building the $CsPbIBr_2$ (001) slab. The experimental results show that doping atoms are only incorporated into the perovskite lattice to a small extent by gradient diffusion.[1] Therefore, we assume that Sn atoms only replace Pb atoms in 4 layers near the interface, and 14 Sn atoms substitute 14 Pb. From the upper layer of $CsPbIBr_2$ to the bottom layer, the proportions of Pb atoms replaced by Sn are 0%, 25%, 50%, and 100%, respectively.

The TiO_2/non-doped $CsPbIBr_2$ and TiO_2/gradient Sn-doped $CsPbIBr_2$ models are illustrated in Fig. 1(a and b), respectively. For a stable heterojunction, the lattice mismatches should be less than 5%. Therefore, the $CsPbIBr_2$ (001) and TiO_2 (110) faces should be large enough. The stoichiometry of the perovskite is $Cs_{32}Pb_{18}Sn_{14}I_{32}Br_{64}$, and the surface lattice constants of the optimized $CsPbIBr_2$ and TiO_2 are given in Table 1. The lattice mismatches in the (u, v) directions for the non-doped and gradient Sn-doped cases were (−2.50%, −2.52%) and (−2.93%, −2.89%), respectively. In addition, a vacuum layer of ∼10 Å along the non-periodic direction is added. The model used is large enough to explore the electronic properties of the interface.[23]

After the interface models were established, geometry optimization (GO) and electronic property calculations were carried out. In the calculations, the outermost surface and subsurface atomic layers at the top and the bottom were fixed, and the other layers were allowed to relax. All the calculations were carried out using the Vienna Ab initio Simulation Package (VASP) software.[24] The generalized gradient approximation (GGA) in the form of Perdew–Burke–Ernzerhof (PBE) was used to express the exchange-correlation energy functional.[25,26] As there are heavy elements in our system, the spin–orbital coupling should have a great effect on electronic properties

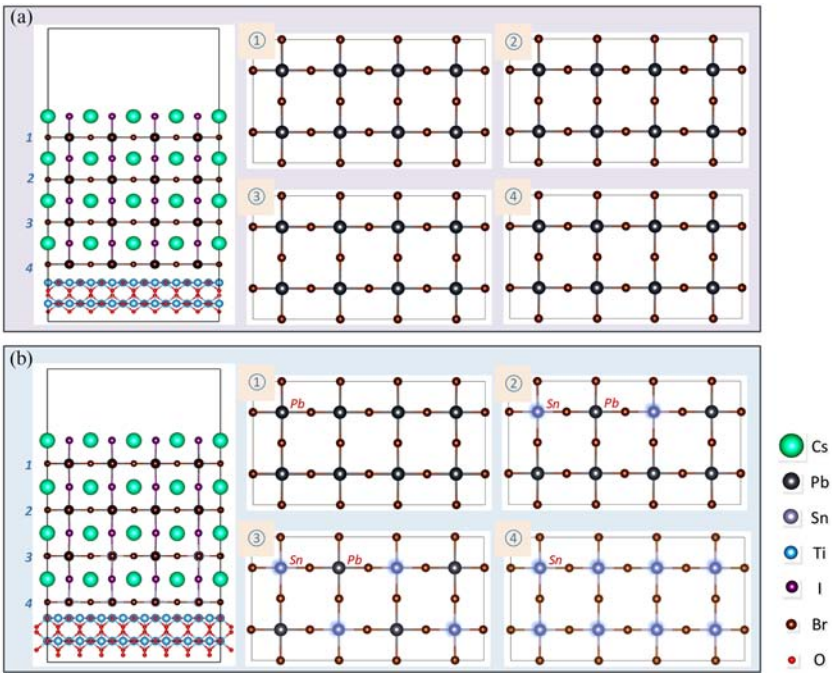

Fig. 1 Structure models of the TiO_2/$CsPbIBr_2$ interface, with (a) non-doped and (b) gradient Sn-doped $CsPbIBr_2$. The atom distributions in each layer are illustrated in sub-images 1–4, respectively.

 This journal is © the Owner Societies 2022

Table 1 Lattice constants, cross-interface bond lengths, and binding energies of the optimized interface models

Interface models	Lattice constants (Å) Before heterojunction: Perovskite	Lattice constants (Å) Before heterojunction: TiO_2	Lattice constants (Å) Heterojunction	Bond lengths (Å)	E_{bind} (eV nm^{-2})
Non-doped $CsPbIBr_2$	u = 23.71 v = 12.51	u = 24.21 v = 12.87	u = 24.21 v = 12.87	Br–Ti 2.81 Pb–O 2.74	−3.534
Gradient Sn-doped $CsPbIBr_2$	u = 23.52 v = 12.25			Br–Ti 2.79 Sn–O 2.61	−3.428

such as the energy band and formation energy;[27] therefore, the SOC effect was considered. To describe the strong electron correlation effect, the Hubbard U correction was used, and the value of U for Ti-3d was set to 3 eV, which has been carefully tested.[28]

The plane wave cut-off energy was set to be 500 eV with a $1 \times 2 \times 1$ Monkhorst–Pack k-point mesh for optimization until the residual stress of each atom was less than 0.01 eV Å^{-1}, and the total energy convergence criterion was 10^{-5}. A $2 \times 2 \times 1$ k-point mesh was used for the calculation of electronic properties.

3. Results and discussion

3.1 Structural stability of the interfaces

The optimized surface lattice constants, u and v, of the $CsPbIBr_2$(001) face with non-doping and gradient Sn-doping are listed in Table 1. They match well with the surface lattice constants of TiO_2(110), which ensures that the perovskite slab can form a stable heterojunction with the TiO_2 slab. The bond lengths and the binding energies between the $CsPbIBr_2$ and TiO_2 slabs were calculated after GO, as shown in Table 1. The shorter Sn–O bonds compared with Pb–O bonds can be attributed to the smaller size of Sn atoms. The binding energy, E_{bind}, is defined as follows:

$$E_{bind} = E_{total} - E_{perovskite} - E_{TiO_2}$$

where E_{total} is the total energy of the interface and $E_{perovskite}$ and E_{TiO_2} are the energies of the perovskite and the TiO_2 slab (with the same configuration as they are in the interface), respectively. It can be seen that these two models are stable, but the TiO_2/non-doped $CsPbIBr_2$ interface is slightly more stable than the TiO_2/gradient Sn-doped $CsPbIBr_2$ interface.

3.2 Enhanced cross-interface electric field

Sn-doping will result in differences in the interfacial charge displacement, thus different cross-interface electric fields. The cross-interface electric field will, in turn, affect the separation of carriers at the interface. The charge density differences (CDDs) of the TiO_2/non-doped $CsPbIBr_2$ and TiO_2/gradient Sn-doped $CsPbIBr_2$ interfaces are shown in the left side of Fig. 2(a and b). The isosurface is set as 0.0095 bohr^{-3}, and the electron accumulation and depletion regions are represented in red and green, respectively. The CDD images show that the electron will be accumulated on the perovskite side while it will be depleted on the TiO_2 side; therefore, an additional electric field from TiO_2 to the perovskite layer will be formed. Such a cross-interface electric field will be helpful for the separation of carriers at the interface.

From the CDD images, we can also observe the different interfacial charge displacements. For the non-doped case (Fig. 2a), the neatest Pb–O bonds will be formed, which indicates that the interfacial charge displacement is the most uniform across the interface. However, in the cases of gradient Sn-doping (Fig. 2b), the interfacial charge displacement becomes complicated, as the chemical environment for the Sn atoms at the interface is not identical due to the atomic

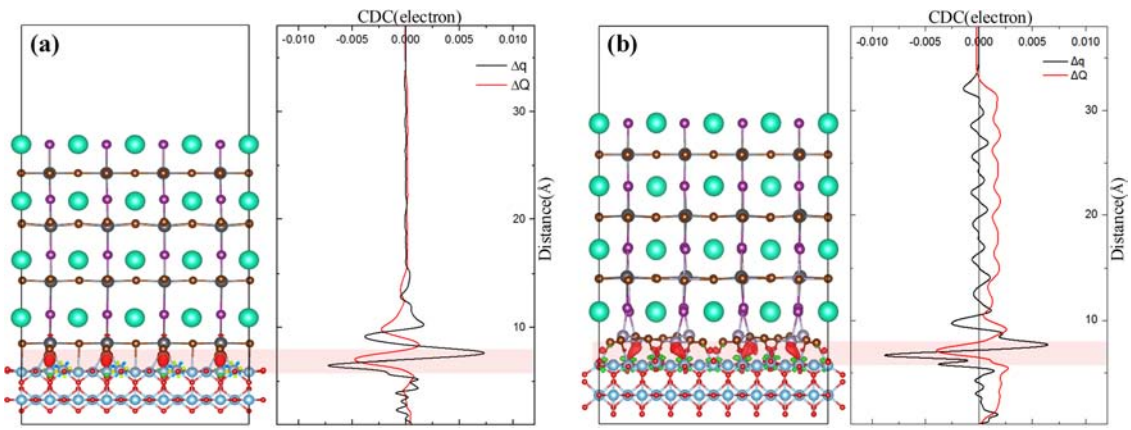

Fig. 2 The optimized models and charge displacement curves of the TiO_2/perovskite interface, with (a) non-doped and (b) gradient Sn-doped $CsPbIBr_2$. In the left side, the region with red and green colors represents electron accumulation and depletion, respectively.

adjustment caused by Sn-doping. About half of the Sn atoms formed Sn–O bonds with the O atoms, which mainly contribute to the interfacial charge displacement.

To quantify the extent of charge displacement across the TiO_2/perovskite interface, we have plotted the charge displacement curves (CDCs) in the right side of Fig. 2(a and b).[29,30] The CDC contains two curves, Δq and ΔQ,

$$\Delta q = \iint (\rho_{TiO_2/perovskite} - \rho_{TiO_2} - \rho_{perovskite}) dx dy$$

$$\Delta Q = \int_0^z \Delta q dz$$

where ρ is the charge density difference, x and y are the directions parallel to the interface, and z is vertical to the interface.[31] Δq indicates the deviation between the charge distribution of the interface and the respective parts (*i.e.*, the TiO_2 and perovskite surface), caused by the charge transfer due to the formation of the interface, where the integration in the x and y directions means that only the distribution of the deviation in the z direction (perpendicular to the interface) is considered. ΔQ stands for the value of the integral of Δq in the z direction, which reflects the accumulation of charges along the z direction.

For both the interface models, the Δq curves have large fluctuations near the interface, which indicates a significant charge transfer at the interface. It can be seen obviously that the electrons are extracted from TiO_2 and accumulated on the perovskite side. Therefore, a built-in electric field is formed from the TiO_2 layer to the perovskite layer.

In the case of gradient Sn-doping, the fluctuations of Δq near the interface are much more significant, which means that the extent of charge displacement across the TiO_2/perovskite interface is enhanced. Meanwhile, with gradient Sn-doping, the values of ΔQ deviate from 0 significantly in regions away from the interface, indicating an intense interface polarization. These two phenomena corroborate, confirming the enhancement of the cross-interface electric field by gradient Sn-doping, which is more conducive to the separation of carriers.[32]

3.3 Optimized bandgap and band matching

The effects of Sn-doping on the carrier separation at the TiO_2/$CsPbIBr_2$ interfaces can be analyzed in more detail based on the density of states (DOS). Fig. 3 shows the DOS of the interfaces and each perovskite layer for both the non-doped and gradient Sn-doped $CsPbIBr_2$ cases. It can be first observed that the existence of the interface affects the band structures of the perovskite layer. The influence range and extent of the interface can be seen from the DOS of each perovskite layer, as shown in Fig. 3c and d. The identifiers 1–4 correspond to those in Fig. 1: layer 4 is the layer closest to the interface. It can be observed that the perovskite layer closest to the interface (layer 4) is more susceptible than other layers. The conductive band energy level of the perovskite layer gradually increases as it moves away from the interface, as does the valence band energy level.

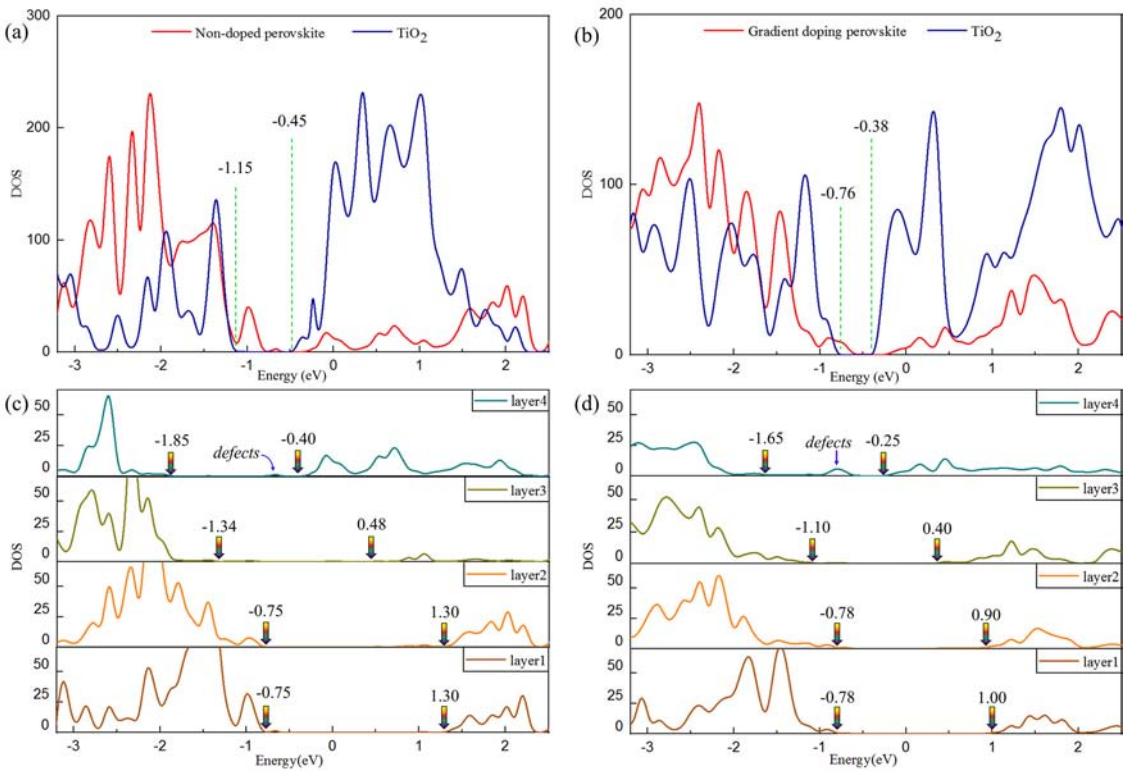

Fig. 3 The DOS of the (a) TiO_2/non-doped perovskite and (b) TiO_2/gradient Sn-doped perovskite interface and of each perovskite layer for the (c) non-doped and (d) gradient Sn-doped cases. Layers 1–4 represent the DOS of perovskite layers 1–4 as shown in Fig. 1.

 This journal is © the Owner Societies 2022

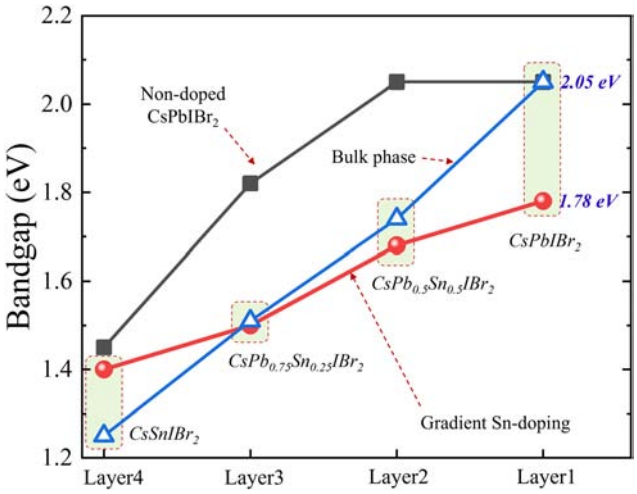

Fig. 4 Bandgaps of each perovskite layer in the interface model and the bulk $CsPb_{1-x}Sn_xIBr_2$.

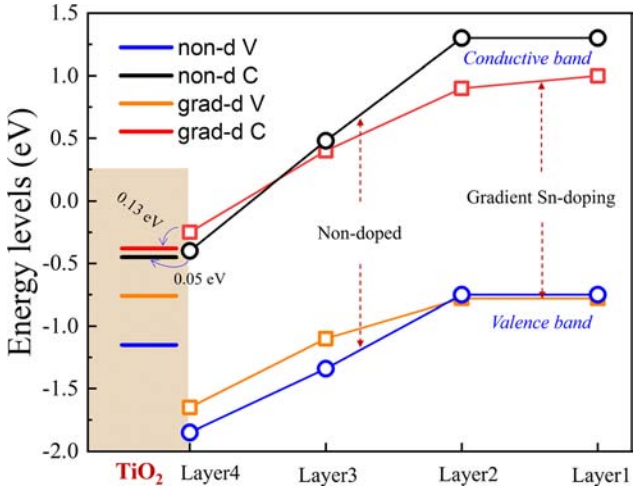

Fig. 5 Band structure at the interface for the gradient Sn-doping and non-doping cases.

However, the increase in the valence band energy level is smaller. As a result, the bandgap of the perovskite layer gradually increases as it moves away from the interface, as shown in Fig. 4. The DOS figures of the 1st and 2nd layers tend to be stable, representing the bulk perovskite. In the non-doped case, the bandgaps of the 1 and 2 layers are both 2.05 eV, which is consistent with that of the bulk $CsPbIBr_2$, 2.05 eV.

Next, we discussed the effect of gradient Sn-doping on the bandgap, the continuity of energy levels, and the resulting electron–hole separation, by comparing the DOS maps of each layer in the case of gradient doping and non-doping. Although the bandgap of the perovskite layer widens from near to far from the interface for both the non-doping and gradient Sn-doping cases, the widening speed and the final value of the bandgap are different in the two cases. At first, in the gradient Sn-doping case, the bandgap of layer 1 is only 1.78 eV, which is significantly smaller than the value of the non-doping case, 2.05 eV, proving that Sn-doping indeed leads to a smaller bandgap.

In addition, in the case of non-doping and gradient Sn-doping, the bandgaps of the perovskite layers 4–1 are 1.45, 1.82, 2.05, and 2.05 eV and 1.40, 1.50, 1.68 and 1.78 eV, respectively. To provide a criterion for the effect of Sn-doping on the bandgap of $CsPbIBr_2$, we have calculated the bandgaps of the bulk $CsPb_{1-x}Sn_xIBr_2$. The obtained bandgaps of the bulk $CsSnIBr_2$, $CsPb_{0.5}Sn_{0.5}IBr_2$, $CsPb_{0.75}Sn_{0.25}IBr_2$, and $CsPbIBr_2$ are 1.25, 1.51, 1.74, and 2.05 eV, respectively. To be more intuitive, we have drawn the bandgaps of each perovskite layer in the interface model and the bulk $CsPb_{1-x}Sn_xIBr_2$ together as shown in Fig. 4. In the case of gradient Sn-doping, the bandgap of each perovskite layer is affected by both the interface and Sn-doping. But for layer 4, maybe because Sn-doping leads to an even smaller interface deformation than the non-doping case (which can be observed in Fig. 2), its bandgap is less affected by the interface. Comprehensively, the bandgap steps between the perovskite layers are smaller and more uniform in the case of gradient Sn-doping.

In both gradient Sn-doping and non-doping cases, the interface effect and Sn-doping will affect the positions of the conduction band and valence band at the same time. In Fig. 5, we plotted the band structure at the interface for the two cases. It can be observed that the gradient Sn-doping will provide more uniform energy steps (the conduction band energy levels of layer 1 to layer 4 are 1.0, 0.9, 0.4, and −0.25 eV, respectively; while in the non-doping case, the values are 1.30, 1.30, 0.48, and −0.40 eV, respectively) for the movement of electrons toward TiO_2. For the transfer of electrons from the perovskite side to the TiO_2 side, in the gradient Sn-doped system, the driving potential, ∼0.13 eV, is also some larger than in the non-doped system, ∼0.05 eV, which is consistent with the stronger interfacial electric field mentioned above.

This work mainly investigated the effect of the interface and Sn-doping on the band structures of the perovskite layers; therefore, only a few TiO_2 layers were used, which had undergone large deformation, as shown in Fig. 1. Consequently, the obtained bandgap of TiO_2 is very different from the experimental results. Besides, Sn-doping will introduce more pronounced defect levels at layer 4, as seen in Fig. 3. This phenomenon may be attributed to the fact that only half of the Sn atoms formed Sn–O bonds with the O atoms in the gradient Sn-doping case, as shown in Fig. 2b. Such additional defects require attention in fabricating Sn-doped $CsPbIBr_2$ solar cells and further experimental investigations.

4. Conclusions

To investigate the impacts of gradient Sn-doping on the carrier separation behaviors at the $TiO_2/CsPbIBr_2$ interface, we have calculated and analyzed the charge displacement and band structures at the $TiO_2/CsPbIBr_2$ interface.

For both the TiO_2/non-doped $CsPbIBr_2$ and TiO_2/gradient Sn-doped $CsPbIBr_2$ interfaces, the electrons will be extracted

from TiO_2 and accumulated on the perovskite side, which means that a built-in electric field from TiO_2 to perovskites is formed. Gradient Sn-doping will bring a larger electron transfer, thus an enhanced cross-interface electric field. Besides, by the impact of the interface, both the conductive and valence band energy levels of the perovskite layer gradually increase as it moves away from the interface; however, the magnitude of the increase in the valence band energy level is minor. Therefore, the bandgap of the perovskite layer gradually increases as it moves away from the interface. In addition, due to the influence of gradient Sn-doping, the steps between the bandgaps of adjacent perovskite layers become smaller and more uniform, and the steps between the conductive band energy levels, *i.e.*, the channel for the extraction of the electron, of adjacent perovskite layers are also smaller and more uniform. In conclusion, from the aspects of the cross-interface electric field, bandgap, and band matching, gradient Sn-doping should be helpful for the electron separation at the $TiO_2/CsPbIBr_2$ interface.

Author contributions

Yingfeng Li conceived of the presented idea, analyzed the results and wrote the manuscript; Bingxin Wang designed the model and carried out the simulation; Yingjian Liu contributed to the drawing of some graphics; Wenxiang Gao corrected the format of the article and the references; and Meicheng Li supervised the findings of this work.

Conflicts of interest

There are no conflicts to declare.

Acknowledgements

This work is supported partially by National Natural Science Foundation of China (Grant no. 52072121, 52232008, 51972110, and 52102245), Beijing Natural Science Foundation (2222076, 2222077), Beijing Science and Technology Project (Z211100004621010), project of State Key Laboratory of Alternate Electrical Power System with Renewable Energy Sources (LAPS202114), the project named key technologies of intelligent joint regulation and operation with grid connected friendly in power station group of wind, solar photovoltaic and energy storage, sponsored by China Three Gorges Corporation (WWKY-2021-0173), 2022 Strategic Research Key Project of Science and Technology Commission of the Ministry of Education, Huaneng Group Headquarters Science and Technology Project (HNKJ20-H88), the Fundamental Research Funds for the Central Universities (2020MS023, 2022MS029, 2022MS02, 2022MS031) and the NCEPU ''Double First-Class'' Program.

Notes and references

1 W. S. Subhani, S. Waqas, K. Wang, M. Y. Du, X. L. Wang and S. Z. Liu, *Adv. Energy Mater.*, 2019, **9**, 1803785.
2 N. J. Jeon, H. Na, E. H. Jung, T. Y. Yang and J. A. Seo, *Nat. Energy*, 2018, **3**, 682–689.
3 H. Tsai, R. Asadpour, J. C. Blancon, C. C. Stoumpos, O. Durand, J. W. Strzalka, B. Chen, R. Verduzco, P. M. A. Jayan and S. Tretiak, *Science*, 2018, **360**, 67–70.
4 Y. Dong, R. Yang, W. Kai, C. Wu, X. Zhu, J. Feng, X. Ren, G. Fang, S. Priya and S. Liu, *Nat. Commun.*, 2018, **9**, 3239.
5 https://www.nrel.gov/pv/assets/pdfs/best-research-cell-efficiencies-rev220126.pdf.
6 L. Zhang, Y. Matsushita, K. Yamaura and A. A. Belik, *Inorg. Chem.*, 2017, **56**, 5210–5218.
7 E. Smecca, Y. Numata, I. Deretzis, G. Pellegrino, S. Boninelli, T. Miyasaka, A. Magna and A. Alberti, *Phys. Chem. Chem. Phys.*, 2016, **18**, 13413–13422.
8 J. Lee, D. Kim, H. Kim, S. Seo, S. M. Cho and N. Park, *Adv. Energy Mater.*, 2015, **5**, 1501310.
9 N. Aristidou, I. Sanchez-Molina, T. Chotchuangchutchaval, M. Brown, L. Martinez, T. Rath and S. A. Haque, *Angew. Chem., Int. Ed.*, 2015, **54**, 8208.
10 L. A. Frolova, D. V. Anokhin, A. A. Piryazev, S. Y. Luchkin, N. N. Dremova, K. J. Stevenson and P. A. Troshin, *J. Phys. Chem. Lett.*, 2017, **8**, 67–72.
11 F. Liu, C. Ding, Y. H. Zhang, T. S. Ripolles, T. Kamisaka, T. Toyoda, S. Hayase, T. Minemoto, K. Yoshino, S. Dai, M. Yanagida, H. Noguchi and Q. Shen, *J. Am. Chem. Soc.*, 2017, **139**, 16708–16719.
12 Q. A. Akkerman, M. Gandini and F. D. Stasio, *Nat. Energy*, 2016, **2**, 16194.
13 Y. Wang, X. Liu, T. Zhang, X. Wang, J. Kan and Y. Zhao, *Angew. Chem., Int. Ed.*, 2019, **58**, 16691–16696.
14 A. Swarnkar, W. J. Mir and A. Nag, *ACS Energy Lett.*, 2018, **3**, 286.
15 Y. Hu, F. Bai, X. Liu, Q. Ji, X. Liu, Q. Ji, X. Miao, T. Qiu and S. Zhang, *ACS Energy Lett.*, 2017, **2**, 2219.
16 Z. Wang, X. D. Liu, Y. W. Lin, Y. J. Lin, Y. J. Liao, Q. Wei and H. R. Chen, *J. Mater. Chem. A*, 2019, **7**, 2773.
17 H. Wang, J. Sun, Y. Gu, C. Xu, Y. Lu, J. Hu, T. Chen, C. Zhu and P. Luo, *Sol. Energy Mater. Sol. Cells*, 2022, **238**, 111640.
18 J. H. Li and Y. X. Yu, *ChemSusChem*, 2021, **14**, 5488–5498.
19 R. Gholizadeh and Y. X. Yu, *J. Phys. Chem. C*, 2014, **118**, 28274–28282.
20 N. Li, Z. Zhu and J. Li, *Adv. Energy Mater.*, 2018, **8**, 1800525.
21 J. Liang, P. Zhao, C. Wang, Y. Wang, Y. Hu, G. Zhu, L. Ma, J. Liu and Z. Jin, *J. Am. Chem. Soc.*, 2017, **139**, 14009–14012.
22 N. Li, Z. Zhu, J. Li, A. K. Y. Jen and L. Wang, *Adv. Energy Mater.*, 2018, **8**, 1800525.
23 S. Zhu, J. T. Ye, Y. Zhao and Y. Qiu, *J. Phys. Chem. C*, 2019, **123**, 20476–20487.
24 G. Kresse and J. Furthmüller, *Comput. Mater. Sci.*, 1996, **6**, 15–50.
25 J. P. Perdew, K. Burke and M. Ernzerhof, *Phys. Rev. Lett.*, 1996, **77**, 3865.
26 P. E. Blöchl, O. Jepsen and O. K. Andersen, *Phys. Rev. B: Condens. Matter Mater. Phys.*, 1994, **49**, 16223–16233.
27 J. H. Li, J. Wu and Y. X. Yu, *J. Phys. Chem. C*, 2020, **124**, 9089–9098.
28 H. Yan, Y. Li, X. Li, B. Wang and M. Li, *RSC Adv.*, 2020, **10**, 958–964.

 This journal is © the Owner Societies 2022

29 E. Ronca, M. Pastore, L. Belpassi, F. Tarantelli and F. D. Angelis, *Energy Environ. Sci.*, 2013, **6**, 183–193.
30 L. Belpassi, I. Infante, F. Tarantelli and L. Visscher, *J. Am. Chem. Soc.*, 2008, **130**, 1048–1060.
31 J. Wang, Y. Huang, J. Guo, J. Zhang, X. Wei and F. Ma, *J. Solid State Chem.*, 2020, **284**, 121181.
32 E. Mosconi, E. Ronca and F. D. Angelis, *J. Phys. Chem. Lett.*, 2014, **5**, 2619–2625.